Spin - Lattice (T_1) and Spin - Spin (T_2) Relaxation

The effect of an RF pulse is to transfer energy from the transmitting coil to the sample protons

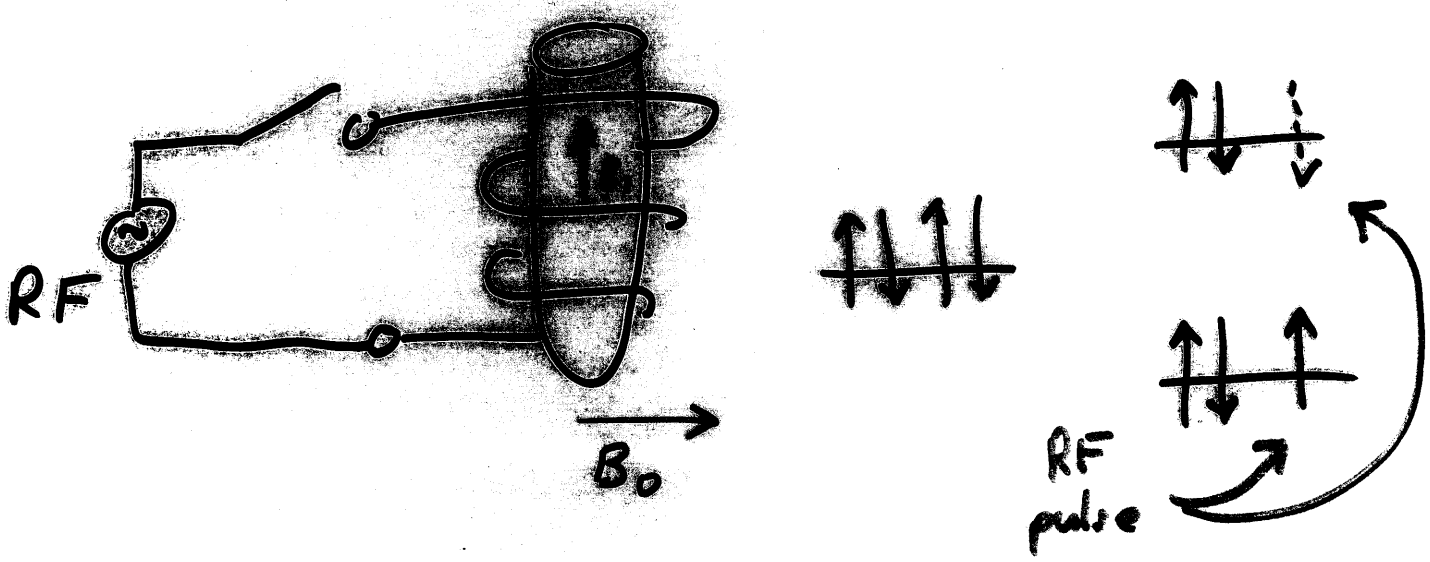

This excess energy results in a non-Boltzmann distribution of the populations of the parallel and the antiparallel energy states.

In the vector model the M_z component has been reduced from its equilibrium value M_0, and the M_x and/or M_y components have a nonzero value. Each of the magnetization components M_z, M_x, and M_y must return to its thermal equilibrium value over time.

The time evolutions of M_z, M_x, and M_y are characterized by differential equations, known as the Bloch equations:

$$\frac{dM_x}{dt} = \gamma M_y \left(B_0 - \frac{\omega}{\gamma} \right) - \frac{M_x}{T_2}$$

$$\frac{dM_y}{dt} = \gamma M_z B_1 - \gamma M_x \left(B_0 - \frac{\omega}{\gamma} \right) - \frac{M_y}{T_2}$$

$$\frac{dM_z}{dt} = -\gamma M_y B_1 - \frac{M_z - M_0}{T_1}$$

The return of M_z to its equilibrium value of M_0 is governed by the spin-lattice (T_1) relaxation time. Immediately after an RF pulse of tip angle α, the M_z component is given by $M_0 \cos\alpha$.

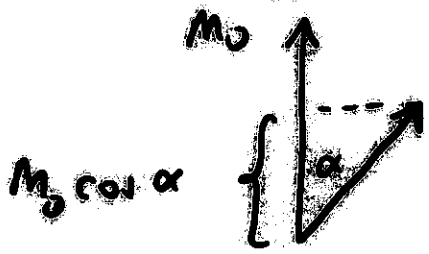

The value of M_z at time t after an RF pulse is given by

$$M_z(t) = M_0 \cos\alpha + (M_0 - M_0 \cos\alpha)(1 - e^{-t/T_1})$$

$$M_z(0) = M_0 \cos\alpha + (M_0 - M_0 \cos\alpha)(1 - 1)$$

$$M_z(0) = M_0 \cos\alpha$$

$$M_z(\infty) = M_0 \cos\alpha + (M_0 - M_0 \cos\alpha)(1)$$

$$M_z(\infty) = M_0$$

If $\alpha = 90^\circ$ (90° or $\pi/2$ tip angle)

$$M_z(t) = M_0\left(1 - e^{-t/T_1}\right)$$

since $\cos \pi_2 = 0$

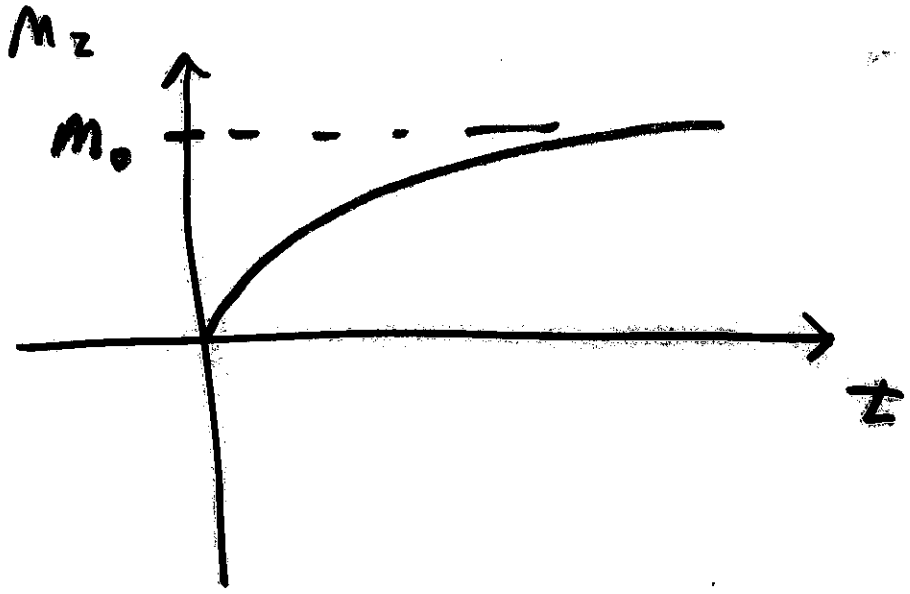

$\pi/2$, pulse

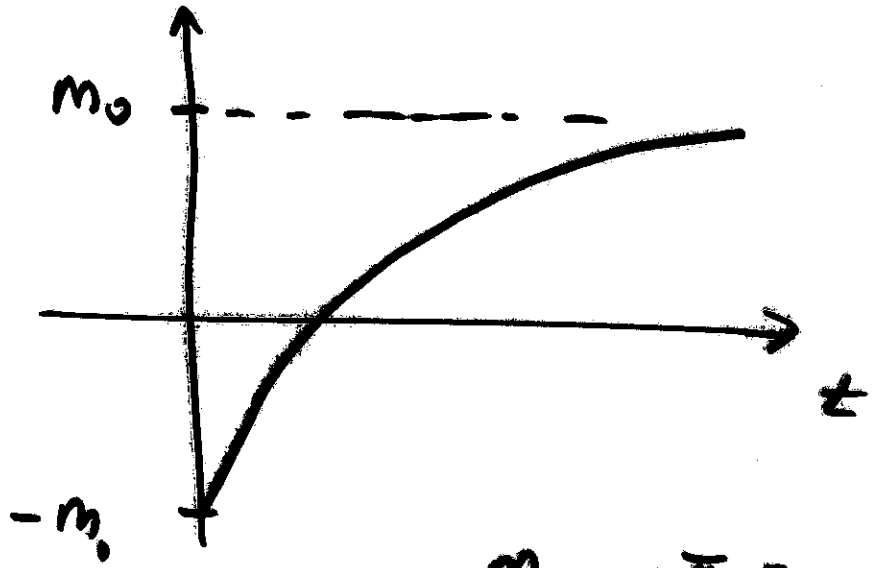

π, pulse

$$M_0 \cos \pi = -M_0$$

$$M_z(t) = -M_0 + (M_0 + M_0)\left(1 - e^{-t/T_1}\right)$$

The physical basis for T_1 relaxation involves protons losing their energy to the surrounding environment (lattice), hence the name spin-lattice relaxation. Different tissues have different T_1 values and this difference forms the basis for tissue contrast in MRI.

T_1 Relaxation Times at 1.5 Tesla

Fat	260 ms
Muscle	870 ms
Brain (Grey)	900 ms
Brain (White)	780 ms
Liver	500 ms
CSF	2,400 ms

The M_x and M_y components of magnetization relax back to their thermal equilibrium values of zero with a time constant termed the spin-spin (T_2) relaxation time:

$$\frac{dM_x}{dt} = -\frac{M_x}{T_2}, \quad \frac{dM_y}{dt} = -\frac{M_y}{T_2}$$

If an arbitrary tip angle α is applied along the x axis, then immediately after the pulse there is no M_x component and the M_y component is given by $M_0 \sin\alpha$.

The value of M_y at time t after the pulse is given by

$$M_y(t) = M_0 \sin\alpha \, e^{-t/T_2}$$

The physical basis of the decay of transverse magnetization is different from the T_1 relaxation process. T_2 relaxation involves the loss of "phase coherence" between the protons precessing in the transverse plane. Even in a perfectly homogeneous B_0 magnetic field, the magnetic moments of different protons precess at slightly different frequencies due to their interactions with neighboring nuclei.

Using the vector model, in the rotating frame

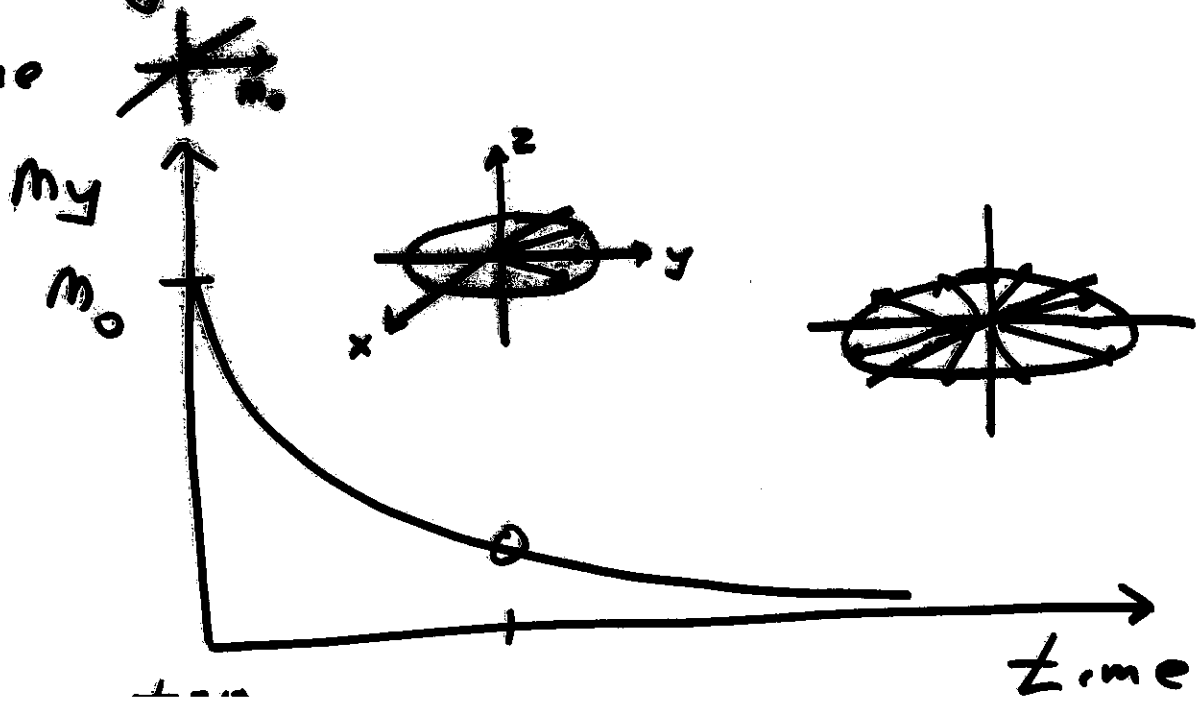

As in the case of T_1, different tissues in the body have different values of T_2, and these can be used to distinguish between soft tissues in clinical MRI.

T_2 Relaxation Times at 1.5 Tesla

Fat	80 ms
Muscle	45 ms
Brain (Gray)	100 ms
Brain (White)	90 ms
Liver	40 ms
CSF	160 ms

In general $T_2 < T_1$

In all practical NMR and MRI systems the loss of phase coherence of the transverse magnetization arises from two different mechanisms. The first is the "pure" T_2 decay as outlined above. The second arises from spatial variations in the strength of the magnetic field. There are two sources of this variation:

1) variations in B_0 in the magnet (impossible to shim perfectly)

2) magnetic susceptibilities vary in tissues (pronounced at air/tissue, bone/tissue boundaries)

Overall

$$\frac{1}{T_2^*} = \frac{1}{T_2'} + \frac{1}{T_2}$$

(ΔB_0)

For $\pi/2$ pulse

$$M_y(t) = M_0 e^{-t/T_2^*}$$

$$= M_0 e^{-t\left[\frac{1}{T_2'} + \frac{1}{T_2}\right]}$$

$$= M_0 \left(e^{-t/T_2'}\right) e^{-t/T_2}$$

In high quality NMR spectrometer T_2' is very small (because the sample is usually small and homogeneous), so

$$M_y(t) \simeq M_0 e^{-t/T_2}$$

However, in MRI $T_2' << T_2$, hence

$$M_y(t) \simeq M_0 e^{-t/T_2^*}$$

Molecular Basis of Relaxation

As previously discussed, when placed in an external magnetic field, individual protons will assume one of two possible orientations. Let Pr_w and Pr_a denote protons aligned <u>with</u> and <u>against</u> the B_0 field.

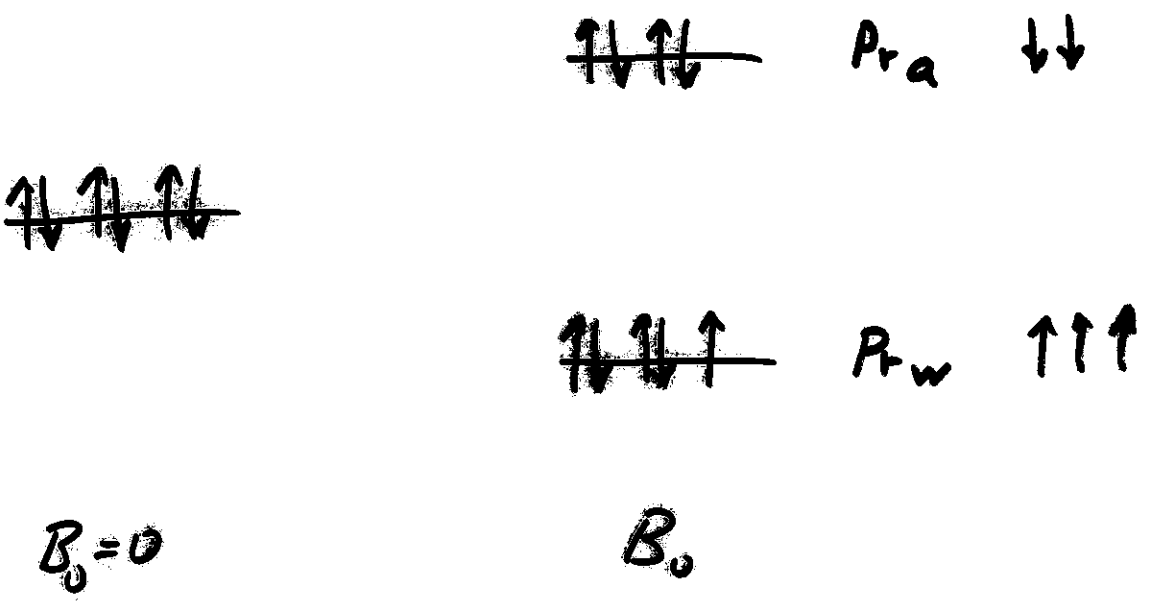

Since the alignment with B_0 is energetically favorable, the transition from Pr_a to Pr_w is more favorable.

The transition between alignment states is analogous to the chemical equilibrium

$$Pr_w \underset{C_r}{\overset{C_f}{\rightleftharpoons}} Pr_a$$

The rate of the forward reaction is equal to $C_f[Pr_w]$ and the rate of the reverse reaction is equal to $C_r[Pr_a]$, for some constants C_f and C_r where the terms in brackets denote concentration. Since the reverse reaction is more favorable $C_r > C_f$.

At equilibrium the forward and reverse reaction rates must be equal, that is,

$$C_f[Pr_w] = C_r[Pr_a]$$

Thus,

$$[Pr_w] = \{C_r / C_a\} [Pr_a]$$

Since $C_r > C_a$ at equilibrium $[Pr_w] > [Pr_a]$ and we have a net excess of protons aligned with B_0 at equilibrium.

However, note that the rate at which equilibrium is achieved is dependent upon the constants C_r and C_a. The greater these constants, the faster equilibrium is achieved.

In addition to their alignment with respect to B_0, the individual protons will themselves precess around the axis of the B_0 field (at $\omega_0 = \gamma B_0$). If a weak B_1 field (in the x-y plane) is present then the B_1 field will tip the proton orientation into the xy plane. This induces a transition from the higher energy state to the lower energy state (and vice versa).

Therefore, the effect of the weak rotating magnetic field on an individual proton is to induce a transition from one alignment state to another.

It is important to note that the small B_1 at ω_0 will induce transitions in both directions.

This is analogous to a catalyst for a chemical reaction. A catalyst serves to increase the rate of both the forward and reverse reactions and therfore increases the rate constants C_f and C_r. This results in an <u>increase</u> in the rate at which equilibrium is achieved, that is, the rotating B_1 field will cause T_1 relaxation!

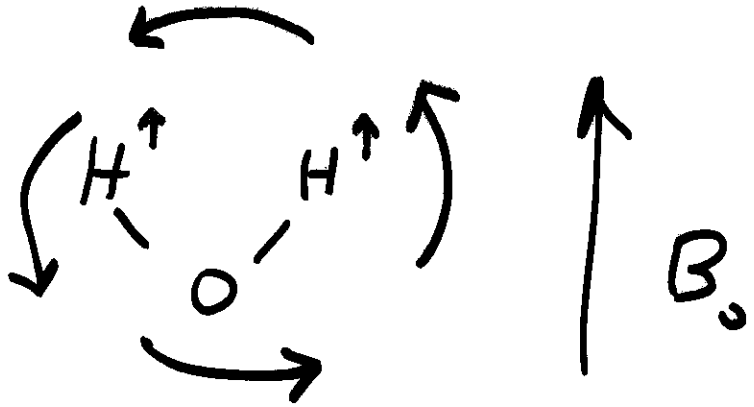

Rotation of H_2O molecule generates rotating B_1!

Note:

1) Only component of B_1 rotating in the x-y plane will induce transitions

2) The rotation of B_1 must be at or near ω_0

3) Since the interaction is between dipoles, the effect occurs only when the dipoles are in close proximity (dipole effect falls off as $1/r^6$!).

Because the effect is due to the interaction of the magnetic field of one proton with another proton - it is usually referred to as <u>proton-proton</u> or dipole-dipole interactions.

$$H_D = \frac{\gamma^2 \hbar^2}{r^3}\left\{ \vec{I}_1 \cdot \vec{I}_2 - \frac{3(\vec{I}_1 \cdot \vec{r})(\vec{I}_2 \cdot \vec{r})}{r^2} \right\}$$

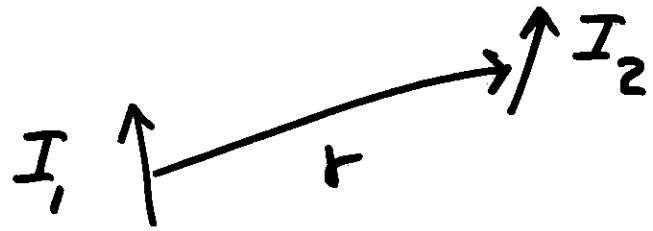

H_D - interaction Hamiltonian

Energy Levels (Two Spin System)

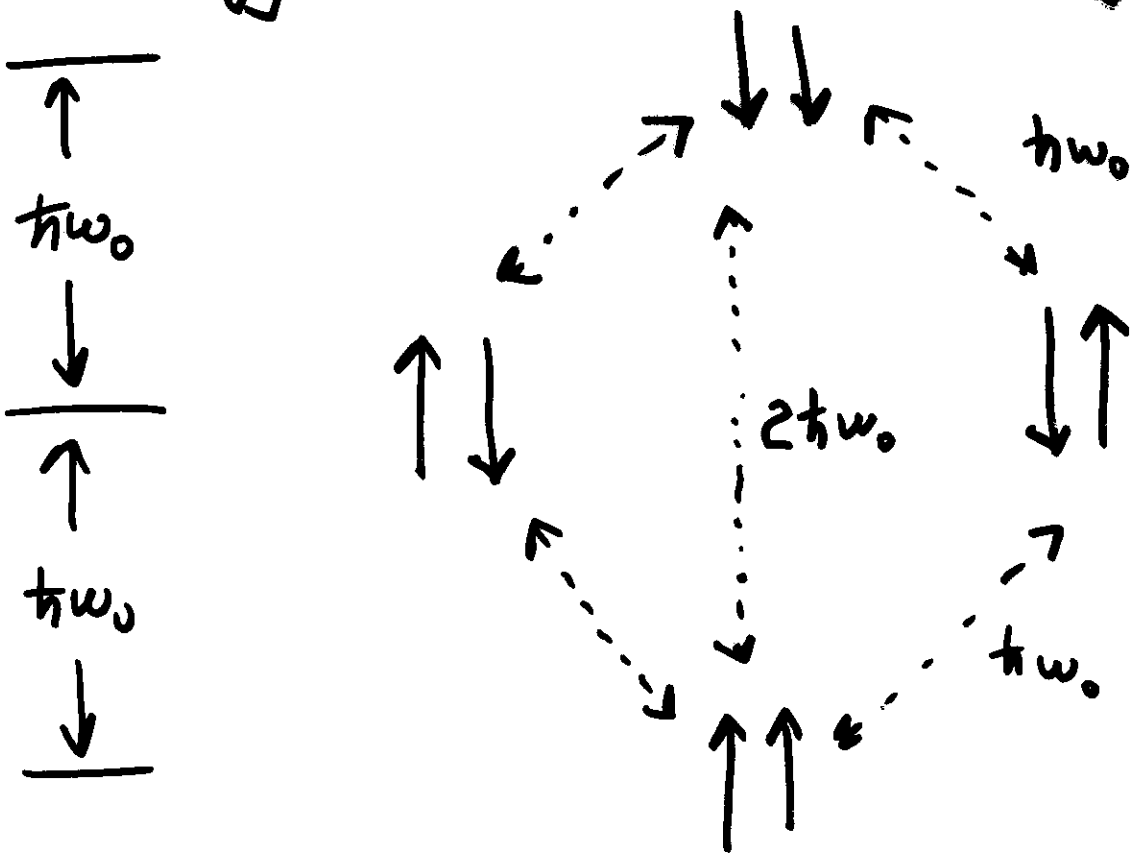

$$\frac{1}{T_1} = \frac{3}{2}\gamma^4\hbar^2 I(I+1)\left\{J_1(\omega_0) + J_2(2\omega_0)\right\}$$

$J_1(\omega)$, $J_2(\omega)$ – spectral density functions

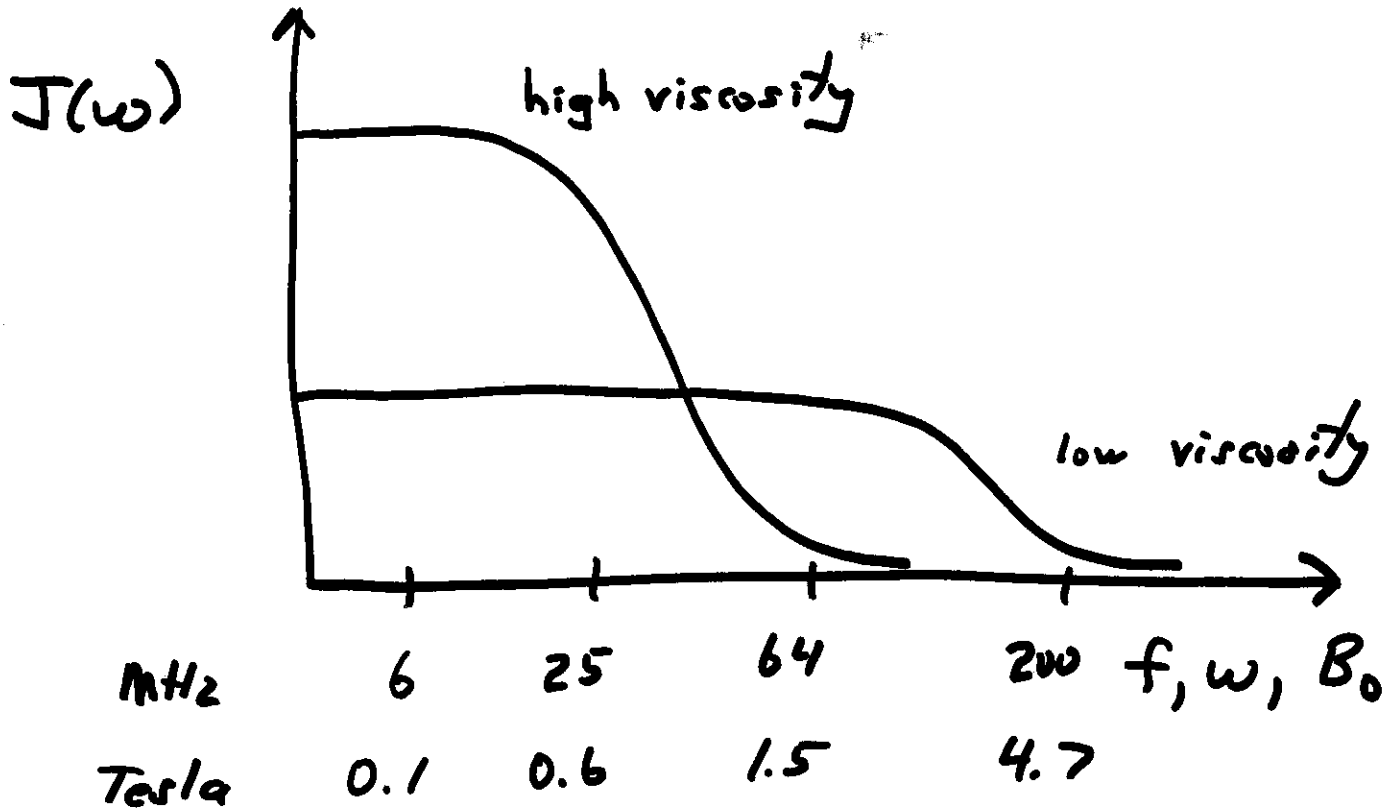

$$J(\omega) \propto \frac{\tau_c}{1+(\omega\tau_c)^2}$$

τ_c – correlation time for interaction

For $\omega\tau_c >> 1$ $\quad \frac{1}{T_1} \propto \frac{1}{\omega^2}$!

Relaxation Models

1) Compartments

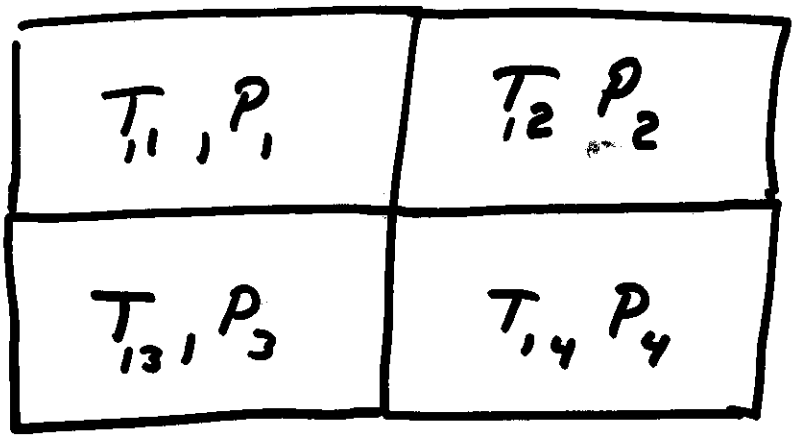

No spin exchange

$$M(t) = M_0 \sum_{i=1}^{n} P_i \, e^{-t/T_{1i}}$$

$n = 2$

$$M(t) = M_0 \left[P_1 e^{-t/T_{11}} + P_2 e^{-t/T_{12}} \right]$$

Example: Breast Tissue

$T_{11} \sim 200$ ms fat

$T_{12} \sim 900$ ms glandular tissue

Rapid Exchange Model

$$M(t) = M_0 e^{-t\left\{\sum_{i=1}^{n} \frac{P_i}{T_{1i}}\right\}}$$

$$\frac{1}{T_1} = \sum_{i=1}^{n} \frac{P_i}{T_{1i}}$$

For $n = 2$

$$M(t) = M_0 e^{-t\left\{\frac{P_1}{T_{11}} + \frac{P_2}{T_{12}}\right\}}$$

$$M(t) = M_0 \left(e^{-t P_1/T_{11}}\right) e^{-t P_2/T_{12}}$$

Bound / Free Water

Most NMR data from tissue makes the assumption that two phases are present: bound water and free water. Bound water is associated with proteins and other macromolecules while free is unassociated. The bound fraction is usually around 10 %.

In the fast exchange model:

$$\frac{1}{T_1} = \left(\frac{1}{T_1}\right)_b P_b + \left(\frac{1}{T_1}\right)_f (1 - P_b)$$

$$\left(\frac{1}{T_1}\right)_b >> \left(\frac{1}{T_1}\right)_f$$

$$\frac{1}{T_1} = \left(\frac{1}{T_1}\right)_f + P_b \left\{ \left(\frac{1}{T_1}\right)_b - \left(\frac{1}{T_1}\right)_f \right\}$$

Spin - Spin Relaxation

$$\frac{1}{T_2} = \gamma^4 \hbar^2 I(I+1)\left\{\frac{3}{8} J_0(0) + \frac{15}{4} J_1(\omega_0) + \frac{3}{8} J_2(2\omega_0)\right\}$$

dipole-dipole for random field fluctuations at $0, \omega_0, 2\omega_0$

$$\frac{1}{T_2} = \frac{\gamma^4 \hbar^2 I(I+1)}{5r^6}\left\{3\tau_c + \frac{5\tau_c}{1+(\omega_0\tau_c)^2} + \frac{2\tau_c}{1+(2\omega_0\tau_c)^2}\right\}$$

$$\frac{1}{T_2^*} = \frac{1}{T_2} + \frac{1}{T_{2\Delta B}} + \frac{1}{T_{2\Delta X}}$$

↑ natural ↑ system ↑ sample

Contrast Agents

Mn^{++}, Gd^{+++}, Fe^{+++} – paramagnetic species

$$\frac{1}{T_1} = \left[\frac{1}{T_1}\right]_0 + k\,[\text{Conc Agent}]$$

k ↑ relaxivity $\left\{\frac{1}{\text{sec-mM}}\right\}$

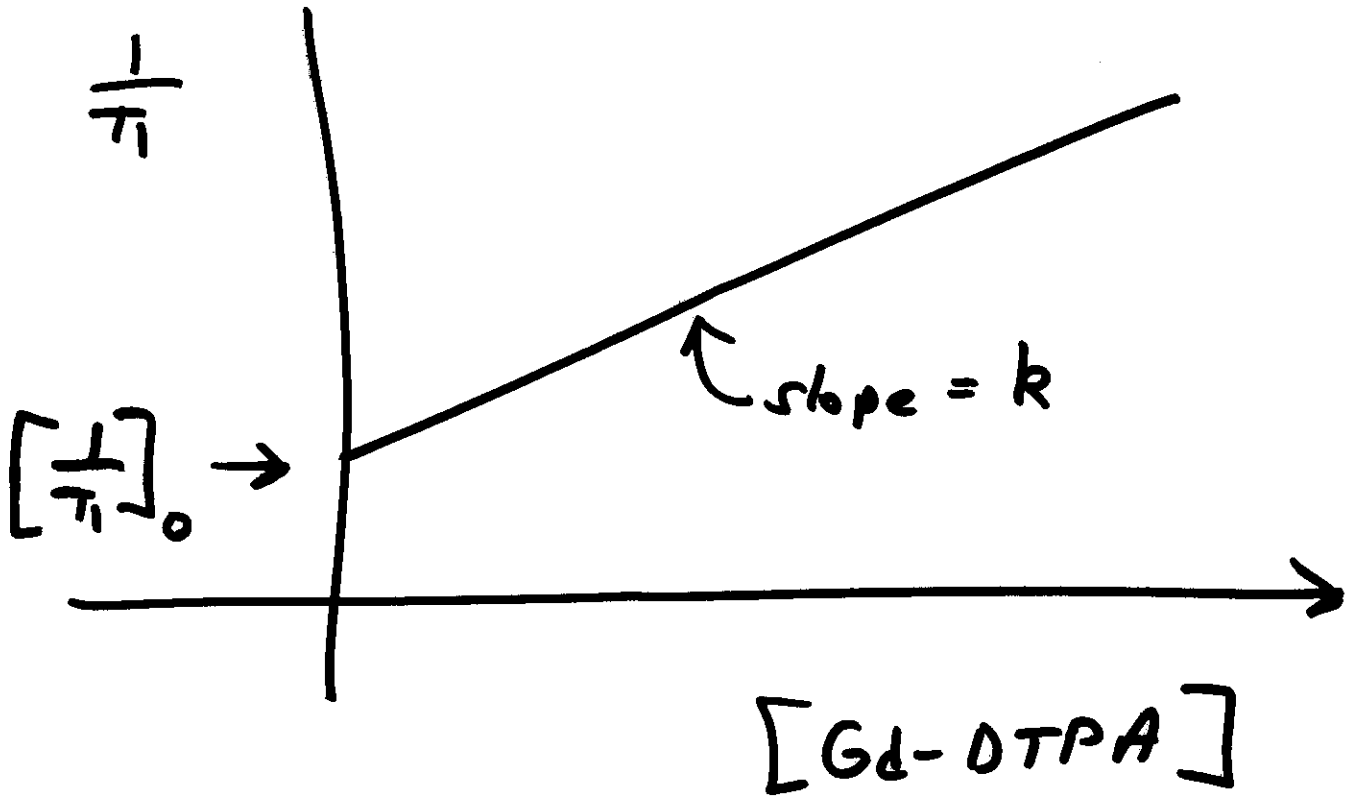

$$M(t) = M_0\left\{e^{-t/T_0}\right\} e^{-tk[\text{Gd-DTPA}]}$$

Relaxation Rate

$$R_1 = \frac{1}{T_1} \quad , \quad R_2 = \frac{1}{T_2}$$

Since $T_1 >> T_2$ (all tissues)

we have $R_1 << R_2$

$T_1 = 500\ ms$, $T_2 = 50\ ms$

$R_1 = 2\ (\frac{1}{s})$, $R_2 = 20\ (\frac{1}{s})$

If Gd-DTPA increases both R_1 & R_2 by 10

$R_1^* = 12$, $R_2^* = 30$

$T_1^* = 83.3\ ms$, $T_2^* = 33.3\ ms$

In clinical MRI Gd-DTPA primarily effects T_1!

NMR Imaging in Biomedicine

P. Mansfield & P.G. Morris

A qualitative indication of this correlation can be seen by comparing the rat-tissue data of Fig. 2.2 (at, say, 100 MHz) with the tissue-water contents of Table 2.1. For instance, liver has a low water content and a short T_1 (high relaxation rate) due to the relatively large fraction of water which is bound, brain and muscle have high water contents, and T_1's and kidney and spleen are intermediate. A more quantitative example is given in Fig. 2.3 which shows the data of Hollis *et al.*[32] both for water content (Fig. 2.3a) and T_1 (Fig. 2.3b), in various normal and malignant rat tissues and is valuable as a reference table of T_1 and water content. Although not strictly applicable to human imaging, the values are close enough to serve as a useful guide. Similar work on rat tissue has been reported by Kiricuta and

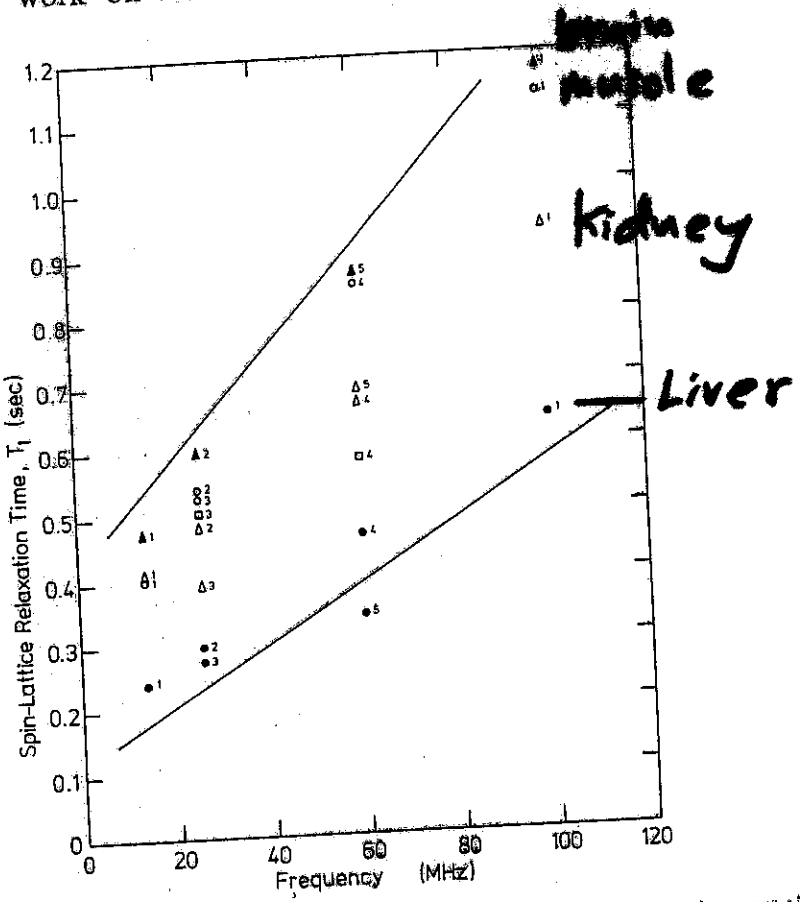

FIG. 2.2. The frequency dependence of spin–lattice relaxation times for various rat tissues: ▲, brain; △, kidney; ●, liver; ○, muscle; □, spleen. Superscripts denote the origin of results: [1]R. E. Block and G. P. Maxwell, *J. Magn. Reson.* **14**, 329 (1974); [2]R. Damadian, *Science* **171**, 1151 (1971); [3]D. P. Hollis, L. A. Saryan, J. C. Eggleston, and H. P. Morris, *J. Natl. Cancer Inst.* **54**, 1469 (1975); [4]W. Bowee, P. Huisman, and J. Smidt, *J. Natl. Cancer Inst.* **52**, 595 (1974); [5]I.-C. Kiricuta, Jr. and V. Simplaceanu, *Cancer Res.* **35**, 1164 (1975).

[32] D. P. Hollis, L. A. Saryan, J. C. Eggleston, and H. P. Morris, *J. Natl. Cancer Inst.* **54**, 1469 (1975).

Simplaceanu.[28] Water contents were measured by weighing and drying the tissues at 100°C for 24 hr. Their results for both T_1 and T_2 are shown in Fig. 2.4a and b and show explicitly the observed relationship between T_1, T_2, and water content for a number of rat tissues. A particularly clear illustration of the linear dependence of T_1 on water content is given in a study by

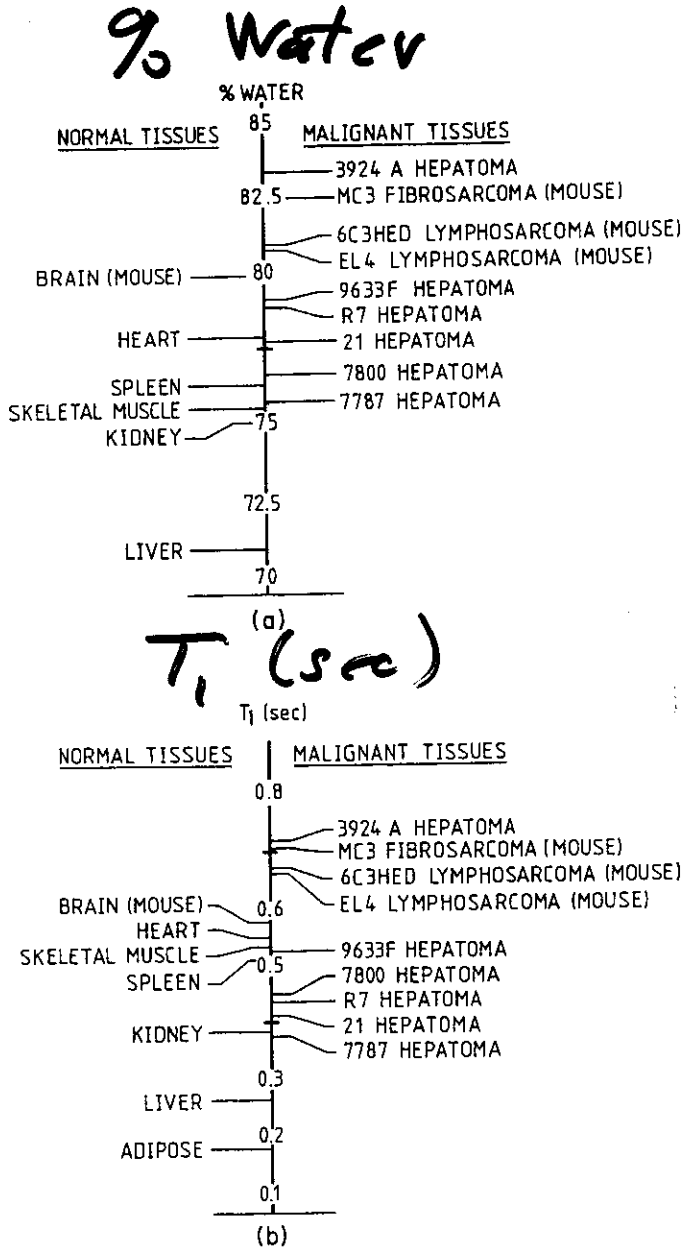

FIG. 2.3. (a) Water content of various normal rat tissues (except mouse brain), and malignant tumors from rats (Morris hepatomas) and mice. (b) Spin–lattice relaxation times T_1 at 24 MHz for various normal rat tissues (except mouse brain) and malignant tumors from rats (Morris hepatomas) and mice. [Both figures taken from D. P. Hollis, L. A. Saryan, and J. C. Eggleston. *J. Natl. Cancer Inst.* **54**, 1469 (1975).]

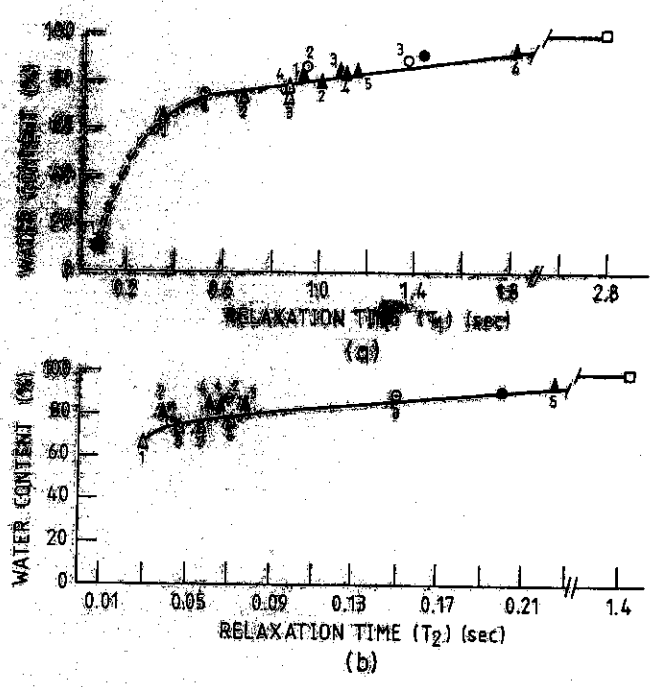

FIG. 2.4. (a) Percent water content versus T_1 for various normal and malignant tissues. (b) Percent water content versus T_2 for various normal and malignant tissues. In both graphs, each point represents the average of values for each tissue type: △, normal tissue [(1) liver, (2) kidney, (3) heart, (4) spleen]; ▲, malignant tissue [(1) lymph node metastasis of Walker 256 carcinoma, (2) Ehrlich solid tumor, (3) Walker 256 carcinoma, (4) Ehrlich ascites (cells), (5) Guerin T_{24}, (6) Ehrlich ascites (cells and liquid)]; ○, immature tissue [(1) liver, (2) heart, (3) brain]; ●, embryo; □, distilled water; ■, dried spleen. [From I. O. Kiricuta and V. Simplaceanu, *Cancer Res.* **35**, 1164 (1975).]

Lauterbur *et al.*[33] of edematous dog lung. (This work was undertaken in order to evaluate the possible use of NMR imaging methods to detect pulmonary extravascular water resulting from systemic or direct lung trauma). These interesting results show quite strikingly what one might describe as a relaxation time amplification effect embodied in our empirical relationship

$$\rho = 0.65 + 0.126T_1 \tag{2.4}$$

obtained from Fig. 2.4a, where T_1 is measured in seconds and ρ is the fractional water content. In its differential form we obtain

$$\Delta T_1 = 7.94\,\Delta\rho \tag{2.5}$$

showing that due to the magnitude of $(1/T_1)_b$, small changes in water content, typically of a few percent, can give rise to large variations in T_1. This

[33] P. C. Lauterbur, J. A. Frank, and M. J. Jacobson, *Dig. Int. Conf. Med. Phys., 4th,* Physics in Canada, **32**, Abstract 33.9 (1976).

$\frac{d\rho}{dT_1} = 0.126 \quad \frac{\Delta T_1}{\Delta\rho} = \frac{1}{.126} = 7.94$

is the basis behind the desire to form NMR images which reflect a T_1 distribution rather than simply spin density. It may be possible to enhance such tissue discrimination by the use of paramagnetic contrast agents such as Mn^{2+} [34] (see Section 2.3.4), allowing one to distinguish between normal, infarcted, and ischemic regions of the heart, for example.

Whereas the water content is generally a good guide to tissue relaxation rates, their strict linear dependence should not be taken too seriously. One might expect that this would hold in a single organ, within narrow physiological limits, but it seems hardly reasonable to expect the relaxation processes to be identical in brain and muscle fiber, for instance! We would not, therefore, dismiss water-content images out of hand. Indeed, our view is that all the NMR parameters, even though they are to a varying extent interrelated, may have some eventual role to play in tissue typing and diagnosis of disease states.

Figure 2.2, which contains data from a number of different sources in the literature, is intended to give the reader a guide to the range and frequency dependence of T_1 values to be expected in healthy animal tissue. The variation in results at 24.3 MHz and at 60 MHz reflects both normal sample variability and the difference in preparative techniques employed by various workers. A more extensive T_1 study of rabbit tissue at 24 MHz has recently been published by Mallard *et al.*[35]

It has been shown that T_1 values for a particular organ generally do not show a great variation with the species of animal.[36] Thus the data of Fig. 2.2 should give a good indication of the values to be expected in humans. That this is approximately correct can be seen by comparing the rat tissue data at 100 MHz with Table 2.2, which lists T_1 values at 100 MHz for human samples (taken from the results of Damadian *et al.*[37]).

With regard to the frequency dependence, in the simplest case of isotropic motion characterized by a single correlation time τ_b, the relaxation rate obeys the well-known modified Bloembergen, Purcell, and Pound (BPP)[38,39] expression

$$\left(\frac{1}{T_1}\right)_b \simeq B\left\{\frac{\tau_b}{1+\omega_0^2\tau_b^2}+\frac{4\tau_b}{1+4\omega_0^2\tau_b^2}\right\}, \tag{2.6}$$

[34] P. C. Lauterbur, M. Helena Mendonca Dias, and A. M. Rudin, Private Communication (1978).

[35] J. Mallard, J. M. S. Hutchison, W. A. Edelstein, C. R. Ling, M. A. Foster, and G. Johnson, *Phil. Trans. R. Soc. London Ser. B* **289**.

[36] G. L. Cottam, A. Vasek, and D. Lusted, *Res. Commun. Chem. Pathol. Pharmacol.* **4**, 495 (1972).

[37] R. Damadian, K. Zaner, D. Hor, and R. DiMaio, *Proc. Natl. Acad. Sci. U.S.A.* **71**, 1471 (1974).

[38] N. Bloembergen, E. M. Purcell, and R. V. Pound, *Phys. Rev.* **73**, 679 (1948).

[39] R. Kubo and K. Tomita, *J. Phys. Soc. Jpn.* **9**, 888 (1954).

TABLE 2.2

T_1 RELAXATION TIMES AT 100 MHz IN NORMAL AND MALIGNANT HUMAN TISSUES[a]

Tissue	Tumor $T_{1\ \text{tumor}}$	Normal $T_{1\ \text{normal}}$	Probability that difference in means are not significant
Breast	1.080 ± 0.08 (13)	0.367 ± 0.079 (5)	0.52×10^{-4}
Skin	1.047 ± 0.108 (4)	0.616 ± 0.019 (9)	0.55×10^{-4}
Muscle:			
Malignant	1.413 ± 0.082 (7)	1.023 ± 0.029 (17)	0.50×10^{-5}
Benign	1.307 ± 0.1535 (2)		
Esophagus	1.04 (1)	0.804 ± 0.108 (5)	
Stomach	1.238 ± 0.109 (3)	0.765 ± 0.075 (8)	0.40×10^{-2}
Intestinal tract	1.122 ± 0.04 (15)	0.641 ± 0.080 (8)[b]	0.27×10^{-5}
		0.641 ± 0.043 (12)[c]	
Liver	0.832 ± 0.012 (2)	0.570 ± 0.029 (14)	
Spleen	1.113 ± 0.006 (2)	0.701 ± 0.045 (17)	
Lung	1.110 ± 0.057 (12)	0.788 ± 0.063 (5)	0.25×10^{-2}
Lymphatic	1.004 ± 0.056 (14)	0.720 ± 0.076 (6)	0.52×10^{-2}
Bone	1.027 ± 0.152 (6)	0.554 ± 0.027 (10)	0.74×10^{-2}
Bladder	1.241 ± 0.165 (3)	0.891 ± 0.061 (4)	0.36×10^{-1}
Thyroid	1.072 (1)	0.882 ± 0.045 (7)	
Nerve	1.204 (1)	0.557 ± 0.158 (2)	
Adipose	2.047 (1)	0.279 ± 0.008 (5)	
Ovary	1.282 ± 0.118 (2)	0.989 ± 0.047 (5)	
Uterus:			
Malignant	1.393 ± 0.176 (2)	0.924 ± 0.038 (4)	
Benign	0.973 (1)		
Cervix	1.101 (1)	0.827 ± 0.026 (4)	
Testes	1.223 (1)	1.200 ± 0.048 (4)	
Prostate	1.110 (1)	0.803 ± 0.014 (2)	
Adrenal	0.683 (1)	0.608 ± 0.020 (5)	
Peritoneum	1.529 (1)	0.476 (1)	
Malignant melanomas	0.724 ± 0.147 (6)		
Tongue	1.288 (1)		
Pericardial layer (mesothelioma)	0.758 (1)		
Kidney		0.862 ± 0.033 (13)	
Brain		0.998 ± 0.016 (8)	
Pancreas		0.605 ± 0.036 (10)	
Heart		0.906 ± 0.046 (9)	

[a] Probability values are reported for series with sample size ≥ 3. Errors reported are standard error of the mean (SEM). Number of cases analyzed are indicated in parenthesis. [From R. Damadian *et al.*, *Proc. Natl. Acad. Sci. U.S.A.* **71**, 1471 (1974).]

[b] Small bowel.

[c] Colon.

where B is a measure of the (usually dipolar) interaction strength and ω_0 is the Larmor frequency. For $\omega_0\tau_b \gtrsim 1$, $(1/T_1)_b$ should vary roughly as ω_0^{-2} and Knispel *et al.*[24] observe this sort of dependence in mouse tissues over the 17–45 MHz region. Note that on the basis of this model, the divergence of T_1 values in Fig. 2.2 at high frequency would seem to indicate a variation in τ_b between the different organs, lending some weight to the view that the tissue T_1 variation is not simply a matter of water content. This divergence also calls into question the often-made assumption that tissue T_1 discrimination improves at lower Larmor frequencies, being optimal at about 2 MHz.[40]

In order to fit adequately the T_1 temperature and frequency variations many workers have found it necessary to introduce a distribution of corre-

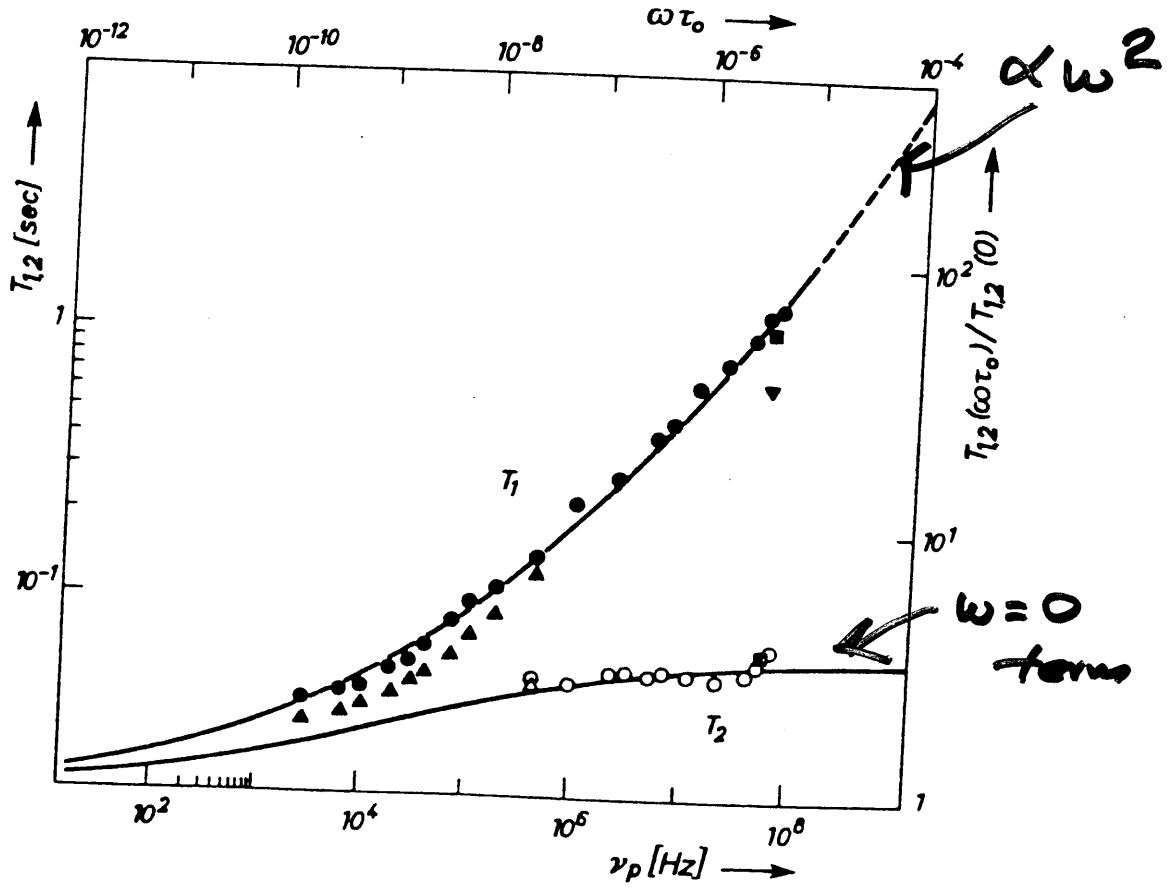

FIG. 2.5. Proton spin–lattice (T_1) and spin–spin (T_2) relaxation times in frog muscle as a function of frequency. (a) *Rana esculenta:* ●, T_1 at 25°C; ▲, T_1 at 0°C; ○, T_2 at 25°C; △, T_2 at 0°C. (b) *Rana pipiens:* ■, T_1 at 25°C; ▼, T_1 at 0°C; □, T_2 at 0 and 25°C. (c) Curves are theoretical fits to Eqs. (3a)–(3c) of Reference 41 with $\tau_0 = 1.1 \times 10^{-14}$ sec, $\alpha = 0.15$, and $T_1(0) = T_2(0) = 1.8 \times 10^{-2}$ sec. [From G. Held, F. Noack, V. Pollak, and B. Melton, *Z. Naturforsch.* **28c**, 59 (1973).]

[40] J. G. Diegel and M. M. Pintar, *J. Natl. Cancer Inst.* **55**, 725 (1975).